

Electronic Supplementary Information

Development of customized 3D printed stainless steel reactors with inline oxygen sensors for aerobic oxidation of Grignard reagents in continuous flow

Manuel C. Maier,^{a,b} René Lebl,^{a,c} Philipp Sulzer,^{a,d} Josef Lechner,^{a,b} Torsten Mayr,^{a,d} Matej Zadavec,^a Eyke Slama,^a Stefan Pfanner,^e Christoph Schmölzer,^f Peter Pöchlauer,^f C. Oliver Kappe,^{a,c} and Heidrun Gruber-Woelfler*^{a,b}

- ^a Center for Continuous Flow Synthesis and Processing (CC FLOW), Research Center Pharmaceutical Engineering GmbH (RCPE), Graz, Austria.
- ^b Institute of Process and Particle Engineering, Graz University of Technology, Graz, Austria.
- ^c Institute of Chemistry, University of Graz, Graz, Austria
- ^d Institute of Analytical Chemistry and Food Chemistry, Graz University of Technology, Graz, Austria.
- ^e Anton Paar GmbH, Graz, Austria
- ^f Patheon Austria GmbH & Co KG, part of Thermo Fisher Scientific, Linz, Austria
- * corresponding author: woelfler@tugraz.at

3D Printing

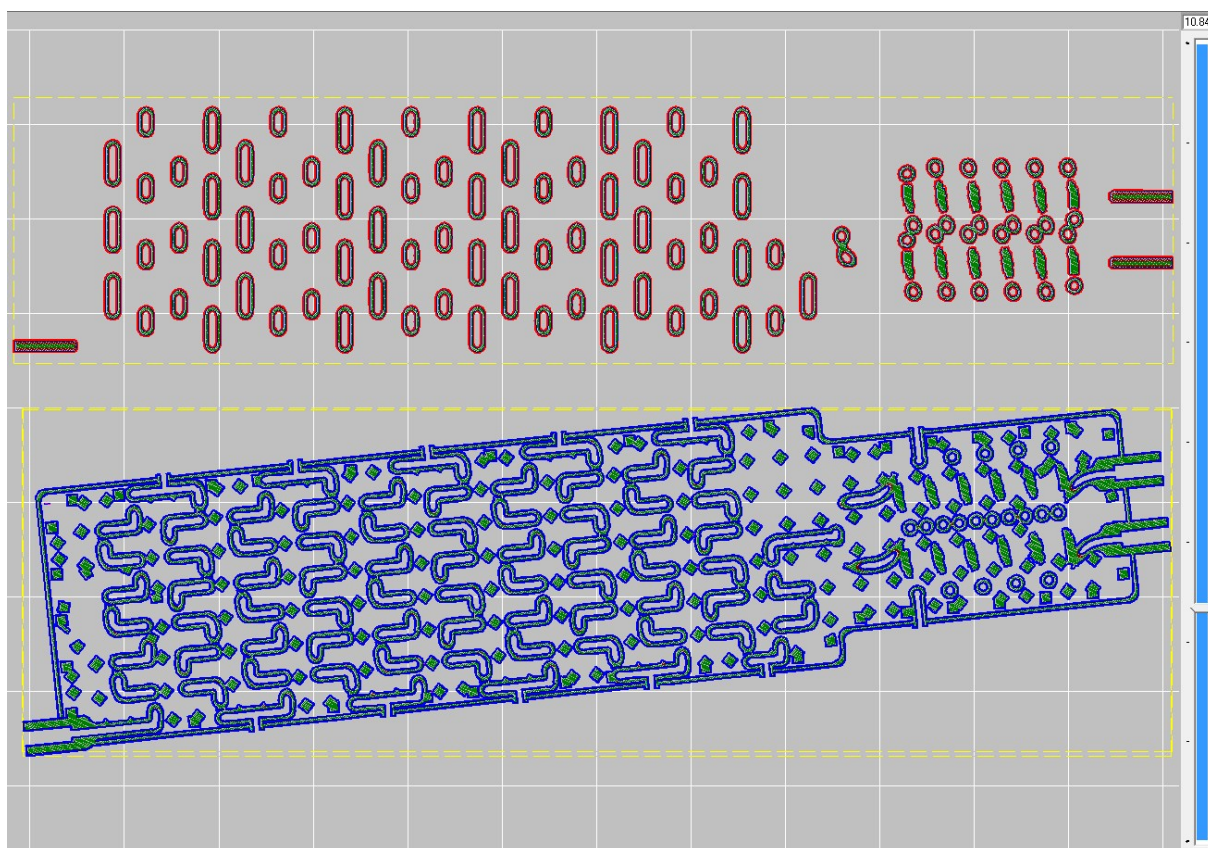


Figure S1: Example of a sliced layer of the split and recombine reactor. For the 3D printing of the reactors, a building layer thickness of 40 μm was chosen and resulted in a total number of 1050 layers. The printing job was done by an SLM system from EOS utilizing an Ytterbium fibre laser with 400 Watt maximum power input. This laser spot scanned through a 316L stainless steel powder bed with a d_{50} of 35.9 μm according to the coloured sliced cross-section areas.

Characterization of the 3D printed reactors

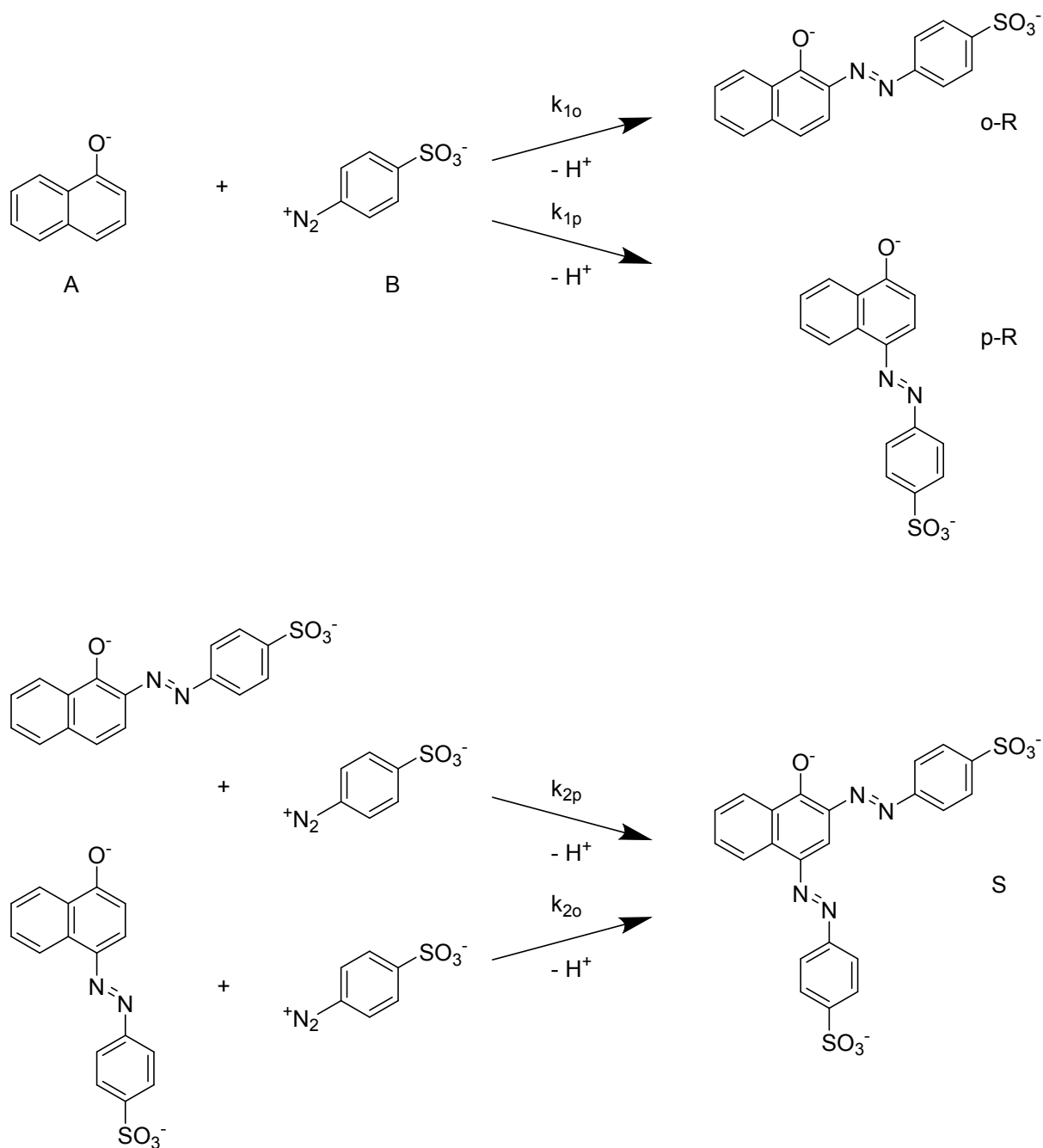


Figure S2: Reaction scheme¹ - diazo coupling of 1-naphthol **A** and diazotized sulphanilic acid **B**. The ortho monoazo dye **o-R** and para monoazo dye **p-R** can further react to the bisazo dye **S**. Influence on the degree of mixing can be seen by the product distribution of this reaction.

Table S1: Molar extinction coefficients of the three dyes published by Bourne et al.¹ at the standard conditions T=25°C, pH 9.9 and I=444.4 mmol L⁻¹. These values were used in the multi-parameter-linear-regression to obtain concentrations of the dyes. Determining separately the concentration of the monoazo dyes was not possible due to overlapping spectra.

wavelength [nm]	Extinction coefficient [m ² mol ⁻¹]		
	p-R	o-R	S
390	277.6	400.6	465.7
400	411.2	395.5	761.3
410	588.7	463.6	972.2
420	794.2	576.6	1246.9
430	1009.6	722.5	1544.1
440	1227.8	901.8	1830.4
450	1456.9	1110.6	2074.9
460	1717.1	1345.8	2245.5
470	2025.7	1611.5	2318.7
480	2382.1	1892.3	2311.7
490	2728.4	2140.4	2246.2
500	3009.6	2317.9	2157.5
510	3158.5	2381.6	2116.9
520	3140.3	2308	2175
530	2959.1	2108.3	2311.4
540	2618.4	1809.4	2467.4
550	2133.5	1431.3	2590.4
560	1583.6	1018.4	2647.4
570	1057.6	638.6	2618.8
580	609.6	343.8	2486.1
590	302.7	166.1	2259.7
600	130.2	74.8	1964.2
610	54.1	35.3	1618.4
620	23.2	15.7	1265.7
630	11.6	8.7	936.1
640	7.9	6.6	652.1
650	4.7	4.2	428.7
660	4.4	4.2	271.9
670	4.1	4.4	161.2
680	2.5	2.7	89.1
690	2.2	2.8	48.9
700	1.6	2.1	28.3

Mixing performance of the CSTR cascade with clockwise and counter clockwise stirrer rotation will be shown in the following. The influence of stirrer RPM and channel flow rate can be seen by the product distribution of the diazo coupling between 1-naphthol and diazotized sulphanic acid. The reaction was started in the cascade's second vessel. Lower yield of product S indicates better mixing. The used stirrer Reynolds numbers $Re(\text{stirrer})$ is calculated with a stirrer diameter of 2.4 mm and the set RPM values of the laboratory magnetic stirrer. Channel Reynolds number $Re(\text{channel})$ is based on the channel diameter of 0.8 mm between the vessels. Experimental errors were checked by calculating a mass balance based on reagent B, which was in depletion. A higher yield of product S led in general to higher experimental errors, whereby a maximum experimental error of 15.5% was found at the lowest flow rate. The mean experimental error of all experiments was close to 4%.

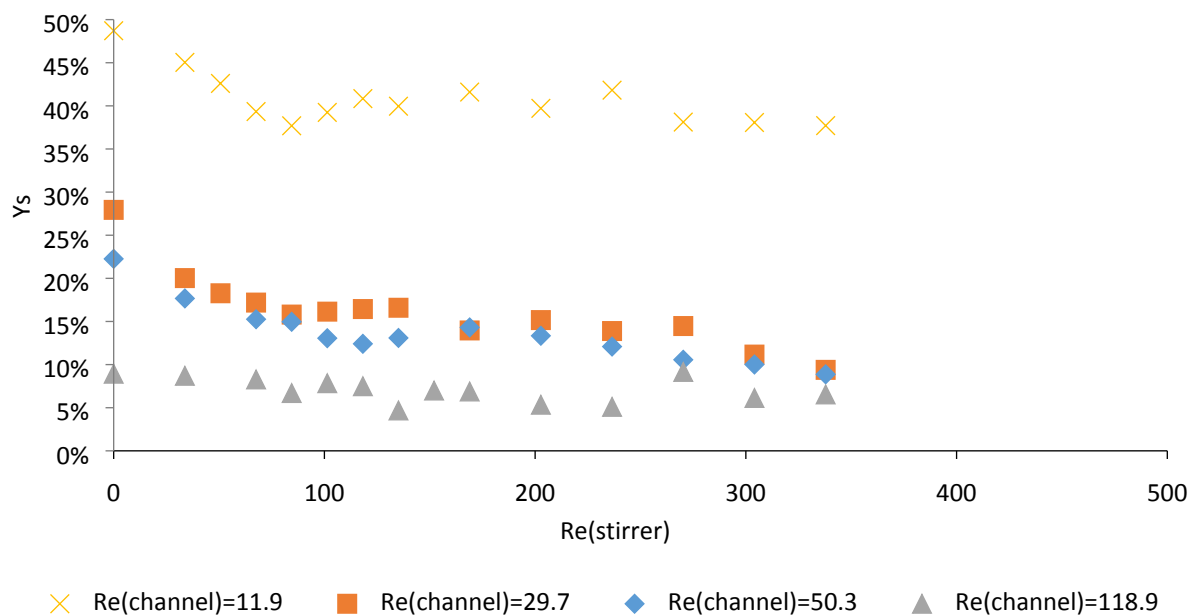


Figure S3: Clockwise stirrer rotation led to a local minimum in the S product yield, indicating a local mixing maximum. This maximum vanishes at higher flow rates. A general trend at higher RPM leading to better mixing can be observed. The influence of RPM on the mixing performance is reduced at higher flow rates.

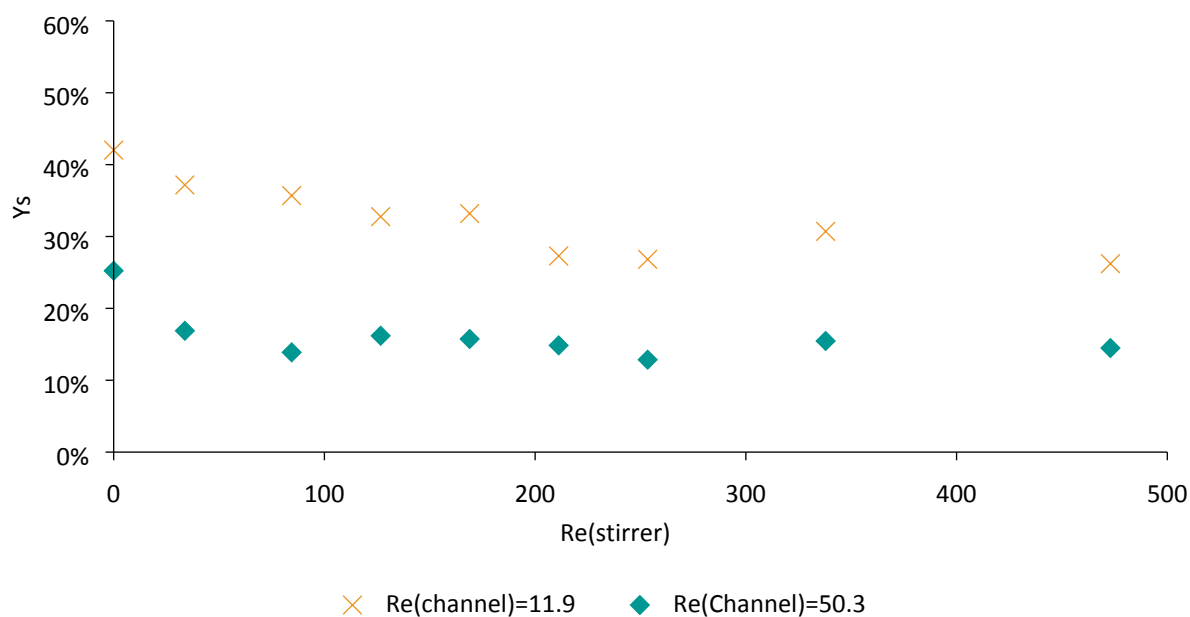


Figure S4: In the counter clockwise operation the local minimum is not present. The general performance of the counter clockwise operation is slightly worse compared to the clockwise operation. Again, the influence of RPM on the mixing performance is reduced at higher flow rates.

Experiments to determine residence time distributions were carried out by an instantaneous step change from solvent (12 w% ethanol in water) to tracer solution (0.006 v% anisole in previously mentioned solvent mixture) while detecting the response of the reactors by an UV/VIS flow cell (10 mm optical path length).

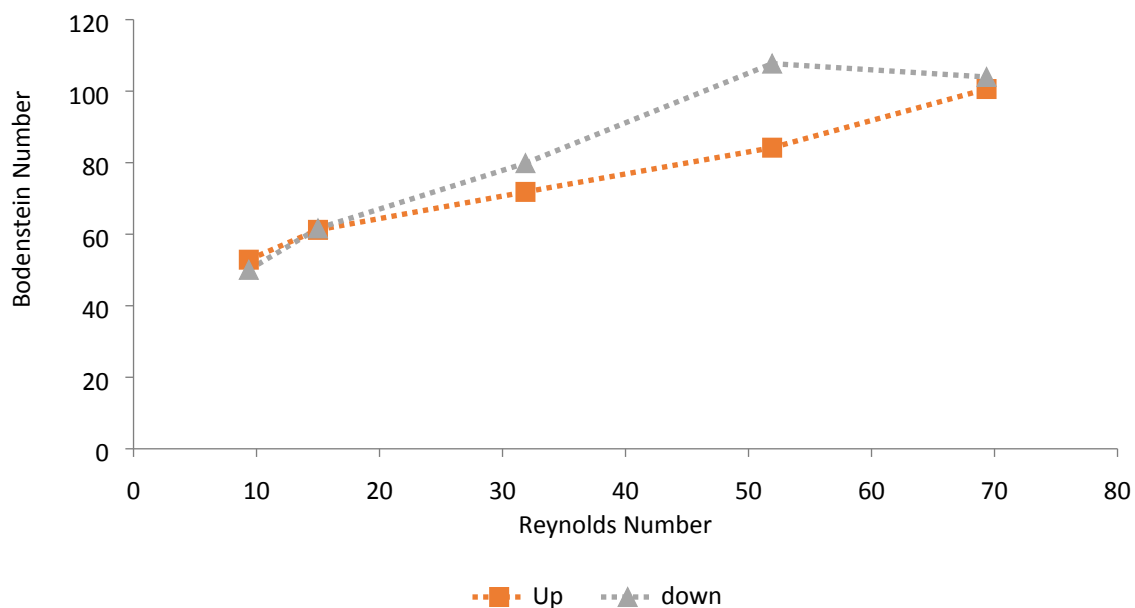


Figure S5: Bodenstein Number for different flow rates in the split and recombine reactor AP02. The steps were performed through one of the reactor feeds while the other one was blocked. A step up means the instantaneous change from solvent to tracer solution and step down the change from tracer solution to solvent. The Reynolds number was calculated with a channel diameter of 0.8 mm and prevailing flow conditions.

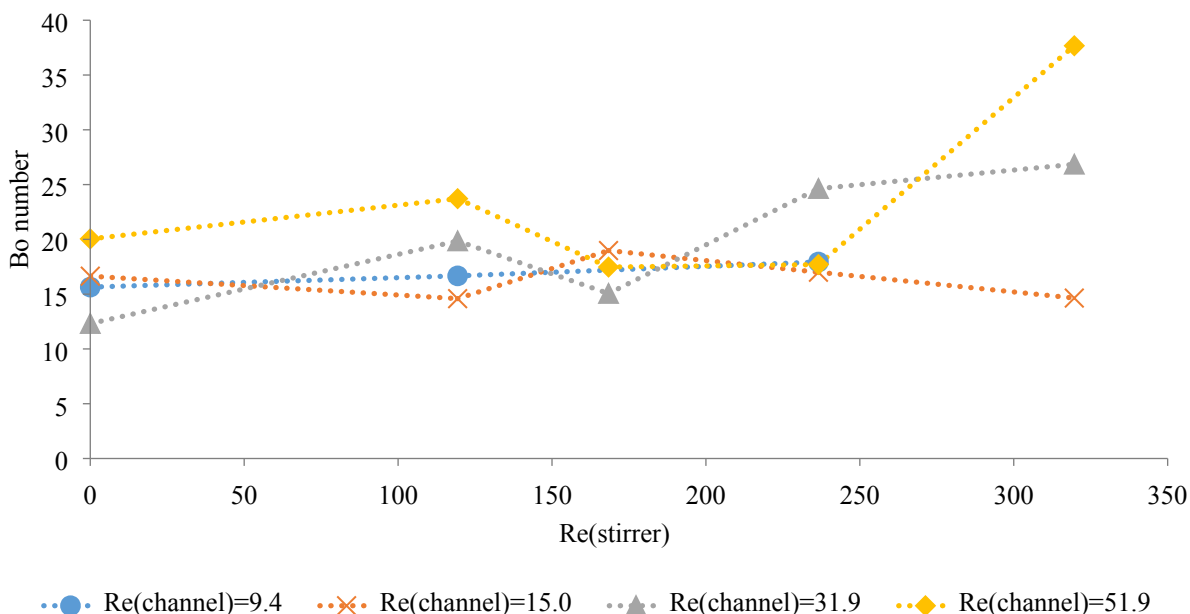


Figure S6: Bodenstein Number for different flow and stirring rates in the CSTR-cascade AP01. This experimental data was obtained for steps up experiment from solvent to tracer solution fed to the first vessel. The Reynolds numbers were calculated with a channel diameter of 0.8 mm for $Re(\text{channel})$, the set RPM value of the magnetic stirrer with a stirrer diameter of 2.4 mm $Re(\text{stirrer})$ and prevailing flow conditions.

Implementation of novel optical oxygen sensors in the set-up



Figure S7: Assembled sensors ready to be implemented into the reactors. A two component epoxy resin was used to attach glass fibres in 1/16" stainless steel tubes which were further glued into HPLC fittings. The sensors were ready to use within the reactor after application of indicator and protection coating.

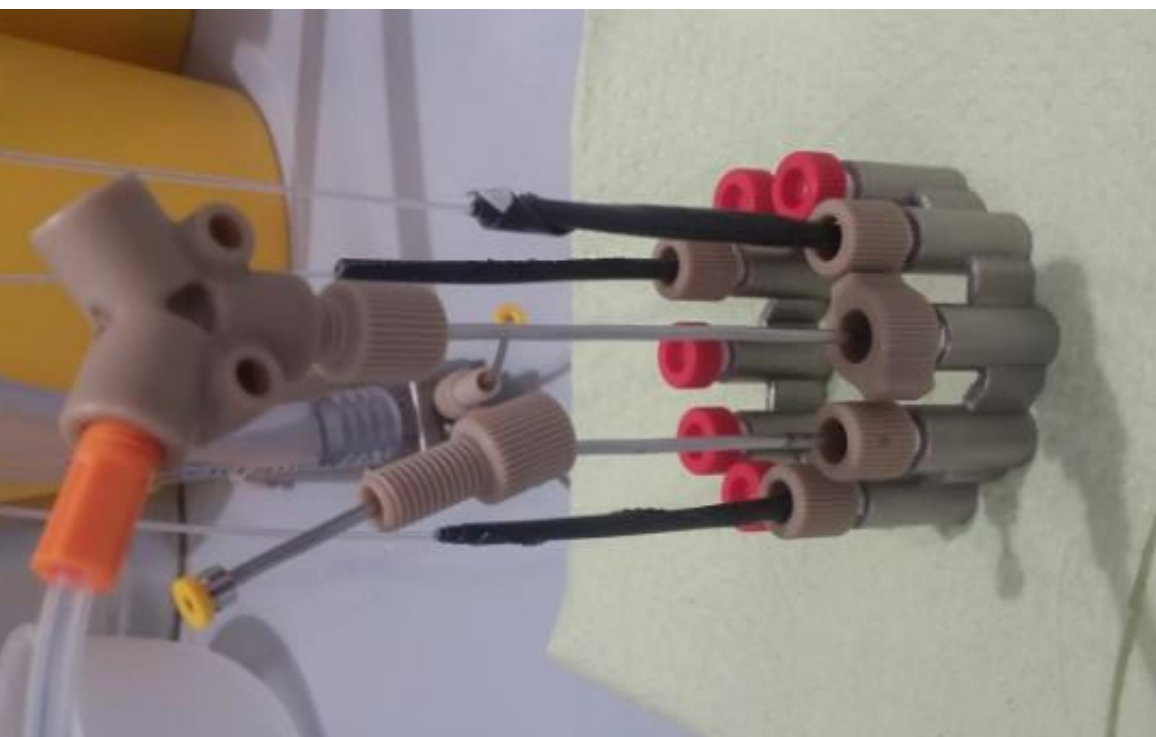


Figure S8: Oxygen sensors integrated in the CSTR cascade AP01. The sensors were carefully screwed into the reactor compartments to prevent breaking of the glass fibre and then connected to the phase fluorimeter readout system. PTFE tape was used to aid proper sealing of the fittings within the pressurized system.

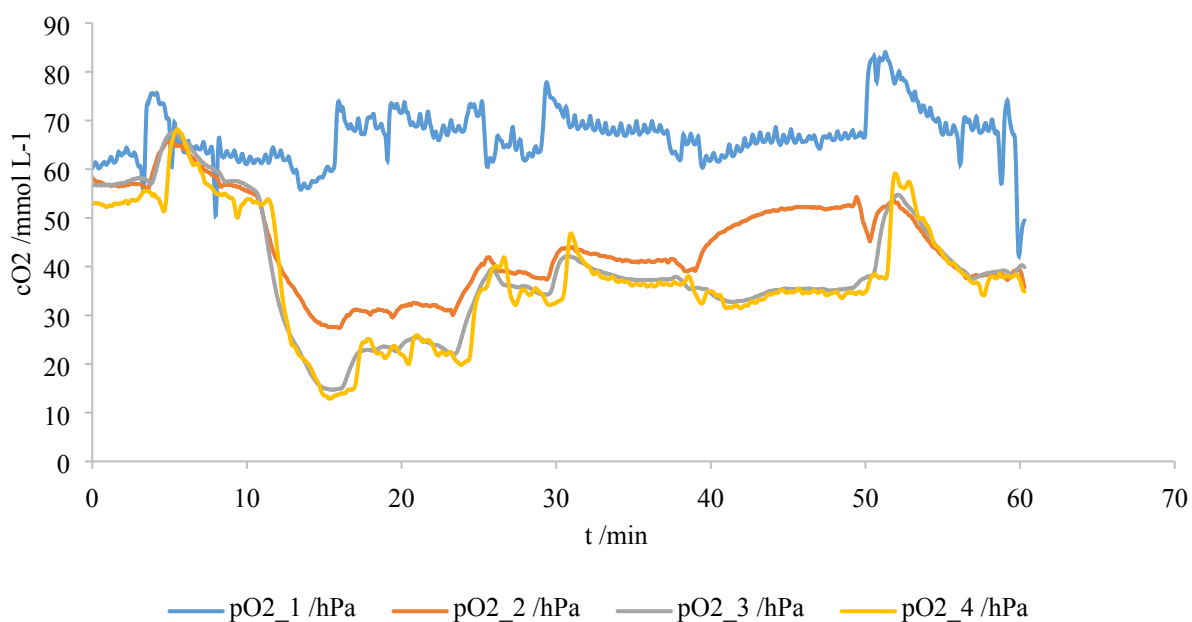


Figure S9: Raw data measured by the oxygen sensors 1 to 4 in the CSTR cascade. This data was collected every six seconds and flattened by calculating the mean value of the last 20 samples. A time correction was done to account for time delays due to different residence times between the sensors. After this correction, it was possible to calculate a relative oxygen concentration as shown in the bottom of figure 10.

Oxidation of Grignard reagents in the novel reactors

Solvents and chemicals were obtained from commercial suppliers and were used without any further purification unless otherwise noted. GC-FID analysis was performed on a ThermoFisher Focus GC with a flame ionization detector, using a TR-5MS column (30 m × 0.25 mm ID × 0.25 μm) and helium as carrier gas (1 mL min⁻¹ constant flow). The injector temperature was set to 280 °C. After 1 min at 50 °C, the temperature was increased by 25 °C min⁻¹ to 300 °C and kept constant at 300 °C for 4 min. The detector gases for flame ionization were hydrogen and synthetic air (5.0 quality). GC-MS spectra were recorded using a ThermoFisher Focus GC coupled with a DSQ II (EI, 70 eV). A TR-5MS column (30 m × 0.25 mm × 0.25 μm) was used, with helium as carrier gas (1 mL min⁻¹ constant flow). The injector temperature was set to 280 °C. After 1 min at 50 °C, the temperature was increased by 25 °C min⁻¹ to 300 °C and kept at 300 °C for 3 min.

Supplementary References

- 1 J. R. Bourne, O. M. Kut, J. Lenzner and H. Maire, *Ind. Eng. Chem. Res.*, 1990, **29**, 1761–1765.